The effect of two-dimensional shear flow on the stability of a crystal interface in a supercooled melt*

Cao Bin(曹 斌), Lin Xin(林 鑫)†, Wang Meng(王 猛), and Huang Wei-Dong(黄卫东)

State Key Laboratory of Solidification Processing, Northwestern Polytechnical University, Xi'an 710072, *China*

(Received 21 December 2011; revised manuscript received 10 February 2012)

A model is developed based on the time-related thermal diffusion equations to investigate the effects of two-dimensional shear flow on the stability of a crystal interface in the supercooled melt of a pure substance. Similar to the three-dimensional shear flow as described in our previous paper, the two-dimensional shear flow can also be found to reduce the growth rate of perturbation amplitude. However, compared with the case of the Laplace equation for a steady-state thermal diffusion field, due to the existence of time partial derivatives of the temperature fields in the diffusion equation the absolute value of the gradients of the temperature fields increases, therefore destabilizing the interface. The circular interface is more unstable than in the case of Laplace equation without time partial derivatives. The critical stability radius of the crystal interface increases with shearing rate increasing. The stability effect of shear flow decreases remarkably with the increase of melt undercooling.

Keywords: spherical crystal, shear flow, interface stability, Trivedi criterion

PACS: 64.70.D–, 64.70.dg, 81.10.Fq, 81.30.Fb **DOI:** 10.1088/1674-1056/21/8/086401

1. Introduction

The solid–liquid interface instability is one of the eternal themes in materials science research. Mullins and Sekerka[1,2] first studied the stability of a solid particle interface. The growth of the interface is controlled by either thermal or solute diffusion. They found that the critical stability radius is seven times the critical radius for nucleation. In reality, the heat and the solute transport processes both should be considered. Trivedi[3] solved this coupled transport problem and obtained a general marginal condition for the absolute shape stability of a spherical particle as

$$-G_{\mathrm{L}} + m_{\mathrm{L}} G_{\mathrm{C}} \xi(l) = (T_{\mathrm{M}} \Gamma / R_0^2) L, \qquad (1)$$

where m_{L} is the slope of the liquidus, G_{L} the temperature gradient, G_{C} the solute gradient, Γ the Gibbs–Thompson parameter, T_{M} the melting point, R_0 the radius of the sphere, l the order of spherical harmonic, $\xi(l)$ and L are each a function of l. In experiment, natural convection or forced stirring can cause liquid flow, which will affect the solute transport significantly. Many researchers studied the relation among liquid flow, solute, and heat transport. Vogel and Cantor[4] investigated the effect of shear flows on the stability of the solid/liquid interface. They found that the shear flows destabilized the solid/liquid interface and favoured the dendritic growth. However the experimental observation showed that shear flows could increase the stability of the solid particles during their free growth.[5,6] To date, the interface stability of a planar interface is still the main focus of most of research. Coriell *et al.*[7] investigated the linear stability of the interface under a plane Couette flow numerically. It was shown that the flow does not affect the wavevectors perpendicular to it, but stabilizes the wavevectors parallel to the flow. Brattkus and Davis[8] analysed the stability of the planar interface under the Stagnation-point flow. They found that the long wavelength perturbations destabilize the interface. Davis and Schulze[9] investigated the effects of steady and oscillatory shear flows on the stability of the interface during directional solidification. They found that the interface is stabilized by the purely oscillatory motion of the crystal in the direction parallel

*Project supported by the National Natural Science Foundation of China (Grant Nos. 50771083 and 50901061), the National Basic Research Program of China (Grant No. 2011CB610402), the Fund of the State Key Laboratory of Solidification Processing in Northwestern Polytechnical University, China (Grant Nos. 02-TZ-2008 and 36-TP-2009), and the Program of Introducing Talents of Discipline to Universities, China (Grant No. 08040).

†Corresponding author. E-mail: xlin@nwpu.edu.cn

© 2012 Chinese Physical Society and IOP Publishing Ltd

to the interface. They further concluded that the appropriate selections of the frequency and amplitude of the modulation can eliminate the morphological instability.[10] Davis and Schulze[11] also found that selecting the flow parameters properly can stabilize the planar interface under the nonparallel shear flows. Lin *et al.*[12] performed a linear stability analysis on a planar interface under the influence of fluid flow. They found that the fluid flow shortens the incubation time for breakdown of the planar interface. Zhao and Li[13] employed the phase-field model to simulate the free dendritic growth process governed by capillary anisotropy or kinetic anisotropy. They discovered that as the interface velocity increases, the cystal radius decreases. Sun *et al.*[14] developed a two-dimensional lattice Boltzmann method-based model for the modelling of dendritic growth during alloy solidification in the presence of forced and natural convections. It is found that convection transports heat and solute from the upstream region to the downstream region, producing asymmetrical dendrite that grows faster in the upstream direction, whereas slower in the downstream direction. Xing *et al.*[15] indicated that there exists a linear relationship between crystal growth velocity and undercooling. As for the spherical interface, Chen *et al.*[16,17] investigated the effect of far-field flow on the crystal growth in the melt. It is shown that the moving velocity of the interface at the upwind side is larger than that on the downwind side. They[18] also found that as the interface kinetic coefficient increases, the growth velocity of the spherical crystal increases.

In our previous work,[19] we used perturbation series to obtain the solutions of temperature field and solute field under far-field flow. In our another paper,[20] the influence of a three-dimensional (3D) shear flow on morphological stability of a globular crystal interface was investigated. We used the Laplace equation modified by material derivatives to solve the temperature and solute fields. However, the influence of the time-dependent diffusion process was neglected in the previous work. In reality, different from the case in planar interface, the surface area of the globular crystal increases with the solidification process, which leads the release of the latent heat and solute (assuming $k_0 < 1$, k_0 is the equilibrium solute distribution coefficient) ahead of the solid/liquid interface to increase with the crystal growth. This means that the thermal and solute diffusion should be time-dependent. In this paper, we focus mainly on the effect of time partial derivatives of the thermal diffusion control equation on the analysis of the morphological stability of the globular crystal of a pure substance in the supercooled melt. We use Ivantsov solution modified by surface energy to represent the temperature field. Since 3D Ivantsov solution is complicated, for simplification, we use a two-dimensional (2D) Ivantsov solution to analyse the solution of temperature field, and investigate the effect of time partial derivative in the diffusion equation on the morphological stability of a 2D circular crystal interface under the shear flow. The growth rate of the interface perturbation amplitude is analysed.

The rest of the present paper is organized as follows. In Section 2, a solution of temperature field for an unperturbed interface growing from a supercooled melt under the shear flows is obtained. We use the time-dependent thermal diffusion equation to solve the temperature field. In Section 3 we present a first order linear stability analysis for the crystal interface. Then we calculate the growth rate of the perturbation amplitude and the critical radius below which the crystal interface is stable. In Section 4 we draw the conclusion from the present study.

2. Theoretical model

The stability analysis of the present paper originates from a phenomenon observed in our previous semisolid solidification experiments.[5,17] We found that the globular crystal radius under stirring is much greater than the radius predicted by classical morphological stability theory based on a pure diffusion condition. The effect of the strong stirring should be a main cause of this remarkable phenomenon. This means that the suitable shear flow of the melt can stabilize the globular crystal significantly. Considering that there is the rotation of globular crystal in suspension in the stirring melt in experiment, we reckon that there should be a shearing flow of certain period around the globular crystal. Since the velocity vector field is hard to solve for a moving globular crystal under stirring, for the purpose of simplifying the analysis, in the present paper, we set the globular crystal to be static and investigate the effect of shear flows on the stability of the spherical interface in an undercooled melt. This flow can be generated by the

rotation of the crystal in the undercooled melt. We assume that the angular velocity of the crystal is ω. To simplify the analysis, we use a rotating frame with an angular velocity ω, thus the crystal becomes static in this rotating frame and the far-field angular velocity of the melt becomes ω. But in the laboratory frame, the angular velocity of the crystal is still ω.

We establish a polar coordinate system in the supercooled melt. The zero point of r axis is the centre of the crystal as shown in Fig. 1. $r = R(\varphi, t)$ can describe the postion and shape of the circular crystal interface. $r = R_0(t)$ represents the interface without the interface perturbation.

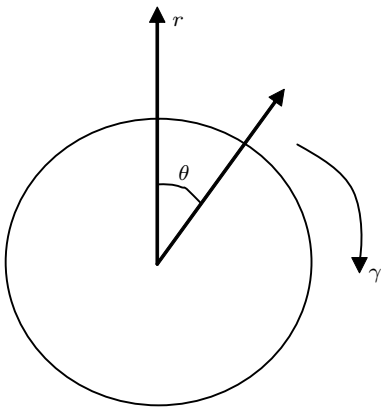


Fig. 1. Shear flow around a crystal. γ represents the shearing rate.

We can use thermal diffusion equations modified by material derivatives to solve the temperature fields:

$$C_{\mathrm{pL}}\frac{\partial T_{\mathrm{L}}}{\partial t} + C_{\mathrm{pL}}\boldsymbol{U}\times\boldsymbol{\nabla}T_{\mathrm{L}} = k_{\mathrm{L}}\Delta T_{\mathrm{L}}, \tag{2}$$

$$C_{\mathrm{pS}}\frac{\partial T_{\mathrm{S}}}{\partial t} + C_{\mathrm{pS}}\boldsymbol{U}_{\mathrm{S}}\times\boldsymbol{\nabla}T_{\mathrm{S}} = k_{\mathrm{S}}\Delta T_{\mathrm{S}}, \tag{3}$$

where T_{L} and T_{S} are the temperatures in liquid and solid, respectively, k_{L} and k_{S} the thermal conductivities in liquid and solid, respectively, C_{pL} and C_{pS} the specific heats of liquid and solid per unit volume, respectively, $\boldsymbol{U}_{\mathrm{S}}$ is the solid-velocity vector, and $\boldsymbol{U}$ the liquid-velocity vector.

The temperature at the interface is determined by the Gibbs–Thomson equation

$$T_{\mathrm{LI}} = T_{\mathrm{SI}} = T_{\mathrm{M}} - \Gamma T_{\mathrm{M}}K, \tag{4}$$

where the subscript I denotes the value at the interface. T_{M} is the equilibrium melting temperature of the pure substance, Γ the capillary constant, K the curvature of the interface.

The temperature at the interface should satisfy the thermal flux conservation condition as follows:

$$-h_{\Delta}\frac{\partial R}{\partial t} = k_{\mathrm{L}}\Big(\frac{\partial T_{\mathrm{L}}}{\partial r}\Big)_{I} - k_{\mathrm{S}}\Big(\frac{\partial T_{\mathrm{S}}}{\partial r}\Big)_{\mathrm{I}}, \tag{5}$$

where $\partial R/\partial t$ is the moving velocity of the interface, h_{Δ} the latent heat of fusion per unit volume.

Since the crystal is relatively static in the rotating frame of reference, then the velocity of the solid particle $\boldsymbol{U}_{\mathrm{S}}$ is

$$U_{\mathrm{S}\varphi} = 0, \tag{6}$$

$$U_{\mathrm{S}r} = 0. \tag{7}$$

Now we use Navier–Stokes equations to obtain the solutions of $\boldsymbol{U}$, expressed as

$$\begin{aligned}&\frac{\partial U_r}{\partial t} + U_r\frac{\partial U_r}{\partial r} + \frac{U_\varphi}{r}\frac{\partial U_r}{\partial \varphi} - \frac{U_\varphi^2}{r}\\ &= -\frac{1}{\rho}\frac{\partial p}{\partial r} + \nu\Big(\frac{\partial^2}{\partial r^2} + \frac{1}{r}\frac{\partial}{\partial r} + \frac{1}{r^2}\frac{\partial^2}{\partial \varphi^2} - \frac{1}{r^2}\Big)U_r\\ &\quad - \nu\frac{2}{r^2}\frac{\partial U_\varphi}{\partial \varphi},\end{aligned} \tag{8}$$

$$\begin{aligned}&\frac{\partial U_\varphi}{\partial t} + U_r\frac{\partial U_\varphi}{\partial r} + \frac{U_\varphi}{r}\frac{\partial U_\varphi}{\partial \varphi} + \frac{U_rU_\varphi}{r}\\ &= -\frac{1}{\rho r}\frac{\partial p}{\partial \varphi} + \nu\Big(\frac{\partial^2}{\partial r^2} + \frac{1}{r}\frac{\partial}{\partial r} + \frac{1}{r^2}\frac{\partial^2}{\partial \varphi^2} - \frac{1}{r^2}\Big)U_\varphi\\ &\quad + \nu\frac{2}{r^2}\frac{\partial U_r}{\partial \varphi},\end{aligned} \tag{9}$$

where ρ is the density of liquid, p the fluid pressure, and ν the kinematic viscosity.

Consider the complexity of solving time-dependent flow field, we assume that $U_r = 0$ and $\boldsymbol{U}$ is related to neither t nor φ. And then the solution of Eq. (9) is

$$U_\varphi = -\gamma R_0^2/2r + \gamma r/2, \tag{10}$$

where

$$\gamma = \left.\frac{\partial U_\varphi}{\partial r}\right|_{r=R_0}$$

is the shearing rate at the interface.

When $r \to +\infty$, U_φ becomes

$$U_\varphi|_{r\to+\infty} = \gamma r/2. \tag{11}$$

The far-field velocity of the undercooled melt is $\omega = \gamma/2$. But since we use a rotating frame, the far-field velocity of the melt is zero in the laboratory frame.

Since $U_r = 0$ and $U_{\mathrm{S}r} = 0$, the shear flow will not affect the temperature fields if they are only related

to r. Equations (2) and (3) become

$$\frac{C_{\rm pL}}{k_{\rm L}}\frac{\partial T_{\rm L}}{\partial t}=\Big(\frac{\partial^2}{\partial r^2}+\frac{1}{r}\frac{\partial}{\partial r}\Big)T_{\rm L}, \tag{12}$$

$$\frac{C_{\rm pS}}{k_{\rm S}}\frac{\partial T_{\rm S}}{\partial t}=\Big(\frac{\partial^2}{\partial r^2}+\frac{1}{r}\frac{\partial}{\partial r}\Big)T_{\rm S}. \tag{13}$$

Using the boundary conditions given by Eqs. (4) and (5), we can solve Eqs. (12) and (13) as follows:

$$T_{\rm S}=T_{\rm M}-T_{\rm M}\Gamma R_0^{-1}, \tag{14}$$

$$T_{\rm L}=\sum_{j=0}^{+\infty}\frac{(r-R_0)^j}{j!}T_j,$$

$$T_0=T_{\rm M}-T_{\rm M}\Gamma r^{-1}, \tag{15}$$

$$T_1=-\frac{h_\Delta}{k_{\rm L}}\boldsymbol{R}_0-T_{\rm M}\Gamma r^{-2}, \tag{16}$$

$$T_2=\frac{h_\Delta}{k_{\rm L}}\frac{C_{\rm pL}}{k_{\rm L}}\boldsymbol{R}_0^2+\frac{h_\Delta}{k_{\rm L}}r^{-1}\boldsymbol{R}_0+T_{\rm M}\Gamma\Big(\frac{C_{\rm pL}}{k_{\rm L}}\boldsymbol{R}_0r^{-2}-2r^{-3}\Big),\cdots, \tag{17}$$

where $R_0(t)=\sqrt{a_1t}$ represents the interface and

$$Ei(x)=\int_{-\infty}^{x}\frac{\mathrm{e}^s}{s}\mathrm{d}s.$$

In Eqs. (15)–(17), we can see that the terms associated with $T_{\rm M}\Gamma$ are also associated with r^{-j} $(j\geq 1)$. When $r\to+\infty$, these terms tend to be zero. Therefore the far-field undercooling $\Delta T_\infty=T_{\rm M}-T_\infty$ can be expressed as

$$\Delta T_\infty=-\frac{a_1h_\Delta}{4k_{\rm L}}\exp\Big(\frac{a_1C_{\rm pL}}{4k_{\rm L}}\Big)\times Ei\Big(-\frac{a_1C_{\rm pL}}{4k_{\rm L}}\Big). \tag{18}$$

We can obtain a_1 from far-field undercooling ΔT_∞ using Eq. (18).

3. Stability analysis

Under the interface perturbation, the interface $R(\varphi,t)$ becomes

$$r=R(\varphi,t)=R_0(t)+\delta(t)\,\mathrm{e}^{\mathrm{i}m\varphi}, \tag{19}$$

where $\delta(t)$ represents the infinitesimal amplitude of the perturbation, m is an integer which represents the perturbation frequency.

The temperature fields influenced by the interface perturbation become

$$T_{\rm L}=\sum_{j=0}^{+\infty}\frac{(r-R_0)^j}{j!}T_j+\delta\,\mathrm{e}^{\mathrm{i}m\varphi}g_1(r), \tag{20}$$

$$T_{\rm S}=T_{\rm M}-\Gamma T_{\rm M}/R_0+\delta\,\mathrm{e}^{\mathrm{i}m\varphi}g_2(r). \tag{21}$$

To obtain the solutions of $g_1(r)$ and $g_2(r)$, we insert Eqs. (20), (21) into Eqs. (2), (3), then we will obtain

$$\boldsymbol{U}\times\boldsymbol{\nabla}(\delta\,\mathrm{e}^{\mathrm{i}m\varphi}g_1)=(k_{\rm L}/C_{\rm pL})\Delta(\delta\,\mathrm{e}^{\mathrm{i}m\varphi}g_1), \tag{22}$$

$$\boldsymbol{U}_{\rm S}\times\boldsymbol{\nabla}(\delta\,\mathrm{e}^{\mathrm{i}m\varphi}g_2)=(k_{\rm S}/C_{\rm pS})\Delta(\delta\,\mathrm{e}^{\mathrm{i}m\varphi}g_2). \tag{23}$$

Equating the coefficients of $\delta\,\mathrm{e}^{\mathrm{i}m\varphi}$ on both sides of the equations, we can obtain

$$\mathrm{i}m\gamma C_{\rm pL}(1-R_0^2r^{-2})g_1/(2k_{\rm L})=\frac{\partial^2}{\partial r^2}g_1+\frac{1}{r}\frac{\partial}{\partial r}g_1-m^2\frac{1}{r^2}g_1, \tag{24}$$

$$\frac{\partial^2}{\partial r^2}g_2+\frac{1}{r}\frac{\partial}{\partial r}g_2-m^2\frac{1}{r^2}g_2=0. \tag{25}$$

Equations (24) and (25) can be solved as

$$g_1(r)=c_0r^b+c_1r^{b+2}+c_2r^{b+4}+\cdots, \tag{26}$$

$$g_2(r)=f_0r^m, \tag{27}$$

$$b=\big[m^2+\mathrm{i}mR_0^2C_{\rm pL}(-\gamma)/(2k_{\rm L})\big]^{1/2},\ \mathrm{Re}(b)<0, \tag{28}$$

$$c_j=\mathrm{i}mC_{\rm pL}\gamma c_{j-1}/\big[2k_{\rm L}(4j^2+4jb)\big],\ (j>0). \tag{29}$$

Using Eq. (4), we can obtain the relationship between g_1 and g_2 as

$$\begin{aligned}&\delta\,\mathrm{e}^{\mathrm{i}m\varphi}\Big(\frac{\partial T_{\rm L}}{\partial r}\Big|_{r=R_0}+g_1\Big|_{r=R_0}\Big)\\&=\delta\,\mathrm{e}^{\mathrm{i}m\varphi}\Big(\frac{\partial T_{\rm S}}{\partial r}\Big|_{r=R_0}+g_2\Big|_{r=R_0}\Big)\\&=\delta\,\mathrm{e}^{\mathrm{i}m\varphi}\Big[-\Gamma T_{\rm M}\Big(K|_{r=R_0+\delta\,\mathrm{e}^{\mathrm{i}m\varphi}}-\frac{1}{R_0}\Big)\Big],\end{aligned} \tag{30}$$

where $g_1|_{r=R_0}=c_0R_0^b+\cdots$, $g_2|_{r=R_0}=f_0R_0^m$.

Inserting Eqs. (20) and (21) into Eq. (5), we can obtain

$$\begin{aligned}&-h_\Delta\dot{\delta}\,\mathrm{e}^{\mathrm{i}m\varphi}\\&=\delta\,\mathrm{e}^{\mathrm{i}m\varphi}\Big[\Big(k_{\rm L}\frac{\partial g_1}{\partial r}\Big|_{r=R_0}-k_{\rm S}\frac{\partial g_2}{\partial r}\Big|_{r=R_0}\Big)\\&\quad+\Big(k_{\rm L}\frac{\partial^2T_{\rm L}}{\partial r^2}\Big|_{r=R_0}-k_{\rm S}\frac{\partial^2T_{\rm S}}{\partial r^2}\Big|_{r=R_0}\Big)\Big].\end{aligned} \tag{31}$$

Insert Eqs. (26) and (27) into Eq. (31), then we will have

$$\begin{aligned}&-h_\Delta\dot{\delta}\,\mathrm{e}^{\mathrm{i}m\varphi}\\&=\delta\,\mathrm{e}^{\mathrm{i}m\varphi}\Big[(k_{\rm L}A_{\nabla T_{\rm L}}g_1|_{r=R_0}-k_{\rm S}A_{\nabla T_{\rm S}}g_2|_{r=R_0})\\&\quad+\Big(k_{\rm L}\frac{\partial^2T_{\rm L}}{\partial r^2}\Big|_{r=R_0}-k_{\rm S}\frac{\partial^2T_{\rm S}}{\partial r^2}\Big|_{r=R_0}\Big)\Big],\end{aligned} \tag{32}$$

where

$$A_{\nabla T_{\rm L}}=\Big(\frac{\partial g_1}{\partial r}\Big|_{r=R_0}\Big)\Big/(g_1|_{r=R_0}), \tag{33}$$

$$A_{\nabla T_{\rm S}}=\Big(\frac{\partial g_2}{\partial r}\Big|_{r=R_0}\Big)\Big/(g_2|_{r=R_0}). \tag{34}$$

Equation (30) contains two separate equations, i.e.,

$$\Big(\frac{\partial T_{\rm L}}{\partial r}\Big|_{r=R_0}+g_1\Big|_{r=R_0}\Big)\delta\,{\rm e}^{{\rm i}m\varphi} = \Big(\frac{\partial T_{\rm S}}{\partial r}\Big|_{r=R_0}+g_2\Big|_{r=R_0}\Big)\delta\,{\rm e}^{{\rm i}m\varphi}, \tag{35}$$

$$\Big(\frac{\partial T_{\rm L}}{\partial r}\Big|_{r=R_0}+g_1\Big|_{r=R_0}\Big)\delta\,{\rm e}^{{\rm i}m\varphi} = -\Gamma T_{\rm M}\frac{m^2-1}{R_0^2}\delta\,{\rm e}^{{\rm i}m\varphi}, \tag{36}$$

where $\dfrac{\partial T_{\rm L}}{\partial r}\Big|_{r=R_0}$ and $\dfrac{\partial T_{\rm S}}{\partial r}\Big|_{r=R_0}$ are caused by the position change of the distorted interface, $g_1|_{r=R_0}$ and $g_2|_{r=R_0}$ are caused by the perturbation of the temperature and solute fields resulting from the distorted interface, and $(m^2-1)/R_0^2$ is the curvature change of the distorted interface.

Inserting Eqs. (35) and (36) into Eq. (32) and equating the coefficients of $\delta\,{\rm e}^{{\rm i}m\varphi}$ on both sides of the equations, the growth rate of the interface perturbation amplitude $\dot\delta/\delta$ can be obtained as

$$\frac{\dot\delta}{\delta} = -v\Big[+(k_{\rm S}A_{\nabla T_{\rm S}}-k_{\rm L}A_{\nabla T_{\rm L}})\Gamma T_{\rm M}\frac{m^2-1}{vh_\Delta R_0^2} + A_{\nabla T_{\rm L}}+\frac{1}{R_0}+\frac{C_{\rm pL}}{k_{\rm L}}v+\frac{T_{\rm M}\Gamma C_{\rm pL}}{h_\Delta R_0^2}\Big]. \tag{37}$$

The imaginary part of $\dot\delta/\delta$ affects the phase change of the interface perturbation. The real part of $\dot\delta/\delta$ represents whether the interface perturbation amplitude becomes larger with time. If $S={\rm Re}(\dot\delta/\delta)>0$, the interface is unstable; if $S<0$, the interface is stable.

When $\gamma=0$, then

$$A_{\nabla T_{\rm L}} = -m/R_0, \tag{38}$$

$$A_{\nabla T_{\rm S}} = m/R_0. \tag{39}$$

Equation (37) becomes

$$\frac{\dot\delta}{\delta} = \frac{G_{\rm L}k_{\rm L}}{h_\Delta R_0}(m-1)\Big[-1-(k_{\rm S}+k_{\rm L})\Gamma T_{\rm M}\frac{m(m+1)}{G_{\rm L}k_{\rm L}R_0^2}+\frac{C_{\rm pL}(T_{\rm M}\Gamma/R_0-R_0G_{\rm L})}{h_\Delta(m-1)}\Big]. \tag{40}$$

where $G_{\rm L}=-h_\Delta v/k_{\rm L}$.

If we set the real part of right-hand side of Eq. (40) to be S_0, then S_0 will determine the stability of the circular crystal interface without flow.

The growth rate of interface perturbation amplitude obtained by Trivedi[3] is

$$\frac{\dot\delta}{\delta} = \frac{k_{\rm L}G_{\rm L}}{R_0h_\Delta}(l-1)\Bigg\{-1-\frac{1}{R_0^2}\frac{T_{\rm M}\Gamma(l+2)}{\dfrac{G_{\rm L}}{l+1+lk_{\rm S}/k_{\rm L}}+\dfrac{m_{\rm L}G_{\rm C}}{-(l+1)+(vR_0/D)(1-k_0)}}\Bigg\}. \tag{41}$$

It can be seen that equations (40) and (41) are similar. The difference results from the fact that Trivedi used a single spherical harmonic $Y_{lm}(\theta,\varphi)=h_{lm}(\theta)\,{\rm e}^{{\rm i}m\varphi}$ to represent the distorted sphere in the 3D case, while we use ${\rm e}^{{\rm i}m\varphi}$ to represent the distorted circular interface in the 2D case. Our analysis focuses on the pure substance and the Trivedi criterion is used for binary melt. Using the time-dependent diffusion equation instead of Laplace equation also induces the difference between our criterion and Trivedi's.

$A_{\nabla T_{\rm L}}$ represents the normal gradient of the liquid temperature field perturbation. Assuming $b\approx -m$, $A_{\nabla T_{\rm L}}$ becomes

$$A_{\nabla T_{\rm L}} \approx -m/R_0+i2h/[R_0(4-4m)] + 2h^2/[R_0(4-4m)^2]+\cdots, \tag{42}$$

where

$$h=\frac{\gamma mC_{\rm pL}R_0^2}{2k_{\rm L}(4-4m)}.$$

The real part of $\dot\delta/\delta$ is affected only by ${\rm Re}(A_{\nabla T_{\rm L}})$ as shown in Eq. (31). The $|{\rm Re}(A_{\nabla T_{\rm L}})|$ in Eq. (42) is obviously smaller than m/R_0. Now we can see that the normal gradient of the liquid temperature field perturbation is reduced compared with the case without flow. When the shearing rate γ increases, the h increases accordingly. We can see from Eq. (42) that the higher order h becomes more significant when h is larger than 1, therefore the effect of shear flow is enhanced. If the shearing rate γ tends to be zero, then the higher order h in Eq. (42) becomes less significant, $A_{\nabla T_{\rm L}}$ will turn into $-m/R_0$ which is the value without flow. The normal gradient of the temperature field perturbation determines the growth rate of the interface perturbation amplitude. Since the shear flow reduces the value of normal gradient of the temperature field perturbation, it also reduces the growth rate of the interface perturbation amplitude, thereby

stabilizing the circular crystal interface.

The effect of time partial derivative of thermal diffusion equations can be represented by the value of $C_{\rm pL}$ on the right-hand side of Eq. (2). The thermal flux conservation at the interface represented by Eq. (5) remains the same.

If the interface perturbation grows faster than the circular crystal interface, then the interface will become unstable. Therefore we use $S' = S - v/R_0$ as the criterion of the stability of the interface. Figure 2 shows the variation of S' with m at an undercooling temperature of 0.5 K and the crystal radius of 100 μm for succinonitrile (SCN). The thermal-physical parameters of SCN are listed in Table 1.[5] It is shown that S' decreases when γ increases. The existence of shear flow reduces the growth rate of the interface perturbation amplitude. We use $m_{\max}$ to represent the value of m when S' reaches its maximum value. It is shown that when γ increases, $m_{\max}$ becomes larger too.

Table 1. Thermal-physical parameters of SCN.

Parameter	Value
$\rho/(\mathrm{kg/m^3})$	1016
$k_{\rm L}/(\mathrm{J/m{\cdot}s{\cdot}K})$	0.222
$k_{\rm S}/(\mathrm{J/m{\cdot}s{\cdot}K})$	0.224
$h_\Delta/(\mathrm{J/m^3})$	4.57×10^7
Γ/m	1.959×10^{-10}
$T_{\rm M}/\mathrm{K}$	331.24
$C_{\rm pL}(\mathrm{J/K/m^3})$	1.9375×10^6

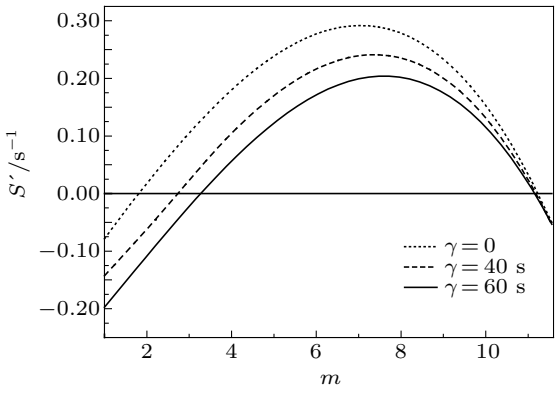


Fig. 2. Curves of S' versus m for $R_0 = 100$ μm and $\Delta T_\infty = 0.5$ K with the different shearing rates.

Calculating the growth rate of the interface perturbation amplitude in Eq. (31), the obtained result contains two parts: (i) the normal gradient of the perturbations of the temperature fields; (ii) the second order partial derivatives of r of the temperature fields which are caused by the position change of the interface. The existence of the time partial derivatives in thermal diffusion equations obviously changes the solution of temperature fields after the occurrence of interface perturbation compared with the case of Laplace equation. That is to say, the time partial derivative in thermal diffusion equation affects the morphological stability of the interface through the second part of the growth rate of the interface perturbation amplitude in Eq. (31), which is caused by the position change of the interface during the interface perturbation.

Figure 3 shows the variations of S' with m for $\Delta T_\infty = 1.0$ K and $R_0 = 100$ μm at different values of $C_{\rm pL}$ and γ. We can see that the growth rate of the interface perturbation amplitude increases with $C_{\rm pL}$. Since $C_{\rm pL}$ is associated with the time partial derivative in thermal diffusion equations, the existence of time partial derivative makes the circular interface more unstable. When we use Lapace equation to study the stability, the interface can tend to be more stable compared with the case with the full form of thermal diffusion equation. $C_{\rm pL}$ represents the heat absorbing ability of the undercooled melt. If $C_{\rm pL}$ is large, the time variation of temperature is slower. The temperature gradient in the melt needs to be larger to change the temperature field with time. Therefore the interface becomes more unstable. We can also see in Fig. 3 that the value of $C_{\rm pL}$ needs to be ten times the normal value $C_{\rm pL} = 1.9375\times10^6$ J/K/m^3 to have a significant effect.

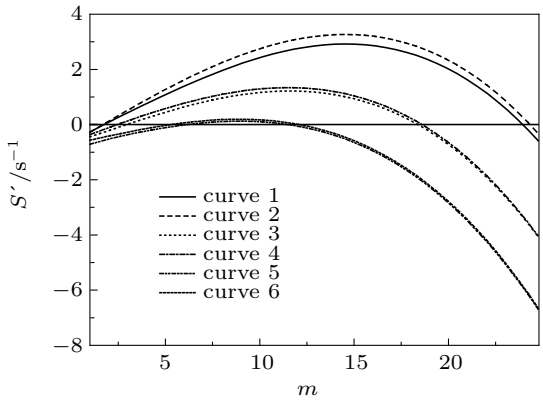


Fig. 3. Curves of S' versus m for $\Delta T_\infty = 1.0$ K and $R_0 = 100$ μm at the different values of $C_{\rm pL}$ and γ: curve 1 $\gamma = 10$ s and $C_{\rm pL} = 2.0\times10^7$ J/K/m^3, curve 2 $\gamma = 0$ and $C_{\rm pL} = 2.0\times10^7$ J/K/m^3, curve 3 $\gamma = 10$ s and $C_{\rm pL} = 1.9375\times10^6$ J/K/m^3, curve 4 $\gamma = 0$ and $C_{\rm pL} = 1.9375\times10^6$ J/K/m^3, curve 5 $\gamma = 10$ s and $C_{\rm pL} = 2.0\times10^5$ /K/m^3, and curve 6 $\gamma = 0$ and $C_{\rm pL} = 1.0\times10^4$ J/K/m^3.

Figure 4 shows the variations of S' with crystal radius R_0. When $\Delta T_\infty = 0.3$ K, the critical stability radii without and with flows are $R_C^* = 30.0$ μm and $R_0 = 32.0$ μm, respectively. Obviously the critical stability radius is larger under the influence of shear flows.

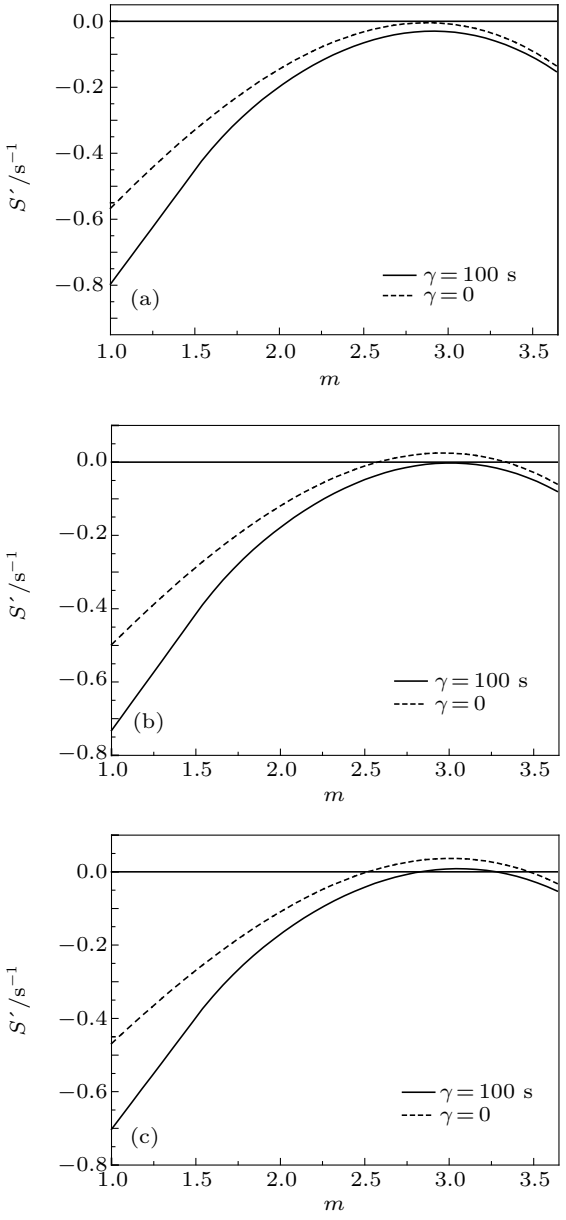


Fig. 4. Curves of S' versus m for $\Delta T_\infty = 0.3$ K at different crystal radii: (a) $R_0 = R_C^* = 30.0$ μm, (b) $R_0 = 1.06$ μm and $R_C^* = 32.0$ μm, (c) $R_0 = 1.1$ μm and $R_C^* = 33.0$ μm.

Figure 5 shows the variations of the critical stability radius with the melt undercooling for the different shearing rates. Since the existence of shear flow can reduce the growth rate of the interface perturbation amplitude, the circular crystal can remain stable with the large radius compared with the case without flow. The critical stability radius increases with shear rate. With or without flow, the critical stability radius becomes smaller when the melt undercooling increases. We can also see from Fig. 5 that the stabilizing effect of the shear flow is insignificant with larger melt undercooling.

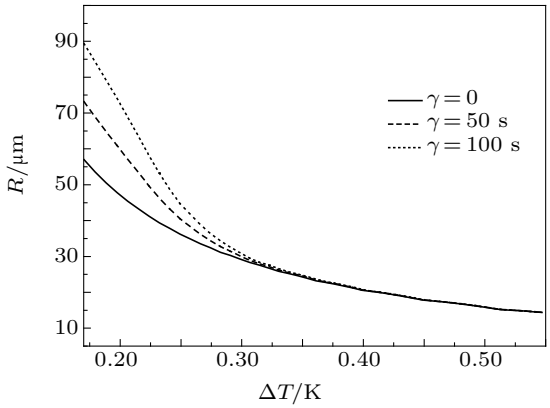


Fig. 5. Curves of critical stability radius R versus ΔT_∞ with the different shearing rates.

4. Conclusion

We develop a model to investigate the effects of 2D shear flow on the stability of a crystal interface in the supercooled melt. In the present model, the time-related diffusion equations instead of Laplace equation are used. The growth rate of the interface perturbation amplitude under shear flow is presented. Similar to the 3D shear flow as described in our previous paper, the 2D shear flow is found to reduce the normal gradient of the perturbations of the temperature fields, which, therefore, can reduce the growth rate of perturbation amplitude. The existence of time partial derivatives of the temperature fields in diffusion equation increases the absolute values of the gradients of the temperature fields, thereby destabilizing the interface, the circular interface is more unstable than the case of Laplace equation without time partial derivatives. The critical stability radius of the crystal interface increases with shearing rate increasing. The stability effect of shear flow decreases remarkably with the increase of melt undercooling.

References

[1] Mullins W W and Sekerka R F 1963 *J. Appl. Phys.* **34** 323

[2] Mullins W W and Sekerka R F 1964 *J. Appl. Phys.* **35** 444

[3] Trivedi R 1980 *J. Crystal Growth* **48** 93
[4] Vogel A and Cantor B 1977 *J. Crystal Growth* **37** 309
[5] Li T, Lin X and Huang W D 2006 *Acta Materialia* **54** 4815
[6] Tong L L, Lin X, Zhao L N and Huang W D 2009 *Acta Metallurgica Sinica* **45** 737
[7] Coriell S R, McFadden G B, Boisvert R F and Sekerka R F 1984 *J. Crystal Growth* **69** 15
[8] Brattkus K and Davis S H 1988 *J. Crystal Growth* **89** 423
[9] Schulze T P and Davis S H 1994 *J. Crystal Growth* **143** 317
[10] Schulze T P and Davis S H 1995 *J. Crystal Growth* **149** 253
[11] Davis S H and Schulze T P 1996 *Metall. Mater. Trans.* **27A** 583
[12] Lin X, Li T, Wang L L, Su Y P and Huang W D 2004 *Acta Phys. Sin.* **53** 3971 (in Chinese)
[13] Zhao D W and Li J F 2009 *Acta Phys. Sin.* **58** 7094 (in Chinese)
[14] Sun D K, Zhu M F, Yang C R, Pan S Y and Dai T 2009 *Acta Phys. Sin.* **58** 285 (in Chinese)
[15] Xing H, Chen C L, Jin K X, Tan X Y and Fan F 2010 *Acta Phys. Sin.* **59** 8218 (in Chinese)
[16] Chen M W, Wang Z D and Xu J J 2007 *Sci. Sin. Tech.* **37** 644
[17] Chen M W, Wang Z D and Sun R J 2007 *Acta Phys. Sin.* **56** 1819
[18] Chen M W, Ni F, Wang Y L, Wang Z D and Xie J X 2011 *Acta Phys. Sin.* **60** 068103 (in Chinese)
[19] Cao B, Lin X and Huang W D 2011 *Acta Phys. Sin.* **60** 066403 (in Chinese)
[20] Cao B, Lin X, Wang M and Huang W D 2011 *J. Crystal Growth* **327** 140